FINAL REPORT

For the doctoral scholarship of the Gesellschaft für Energie und Klimaschutz Schleswig-Holstein GmbH (EKSH)

Carried out at the Fachhochschule Kiel in partnership with the Helmut Schmidt Universität Hamburg

---

Optimization of Aerodynamic Profiles for Wind Turbine Blades by Means of Numerical Simulation with Natural Inflow Turbulence at High Reynolds Numbers

---

Grant Recipient

M.Sc. Brandon Arthur Lobo

Supervisors

Prof. Dr. rer. nat. Alois Schaffarczyk (FH Kiel)

Univ.-Prof. Dr.-Ing. habil. Michael Breuer (HSU Hamburg)

Kiel, 28th June, 2021

1 Introduction

Schleswig-Holstein is the federal state with the largest share of wind energy in Germany. Almost 80 % of the net electricity consumption (in 2015) is covered by its own energy generation from wind power. This makes further development and research on wind turbine blades a very important topic for Schleswig-Holstein. Morever, wind energy supplied 15% of the electricity demand of the European Union in 2019 [1]. Since rotor blades are the determining component for both performance and loads, they are the objective of further optimizations. This objective has gained renewed urgency due to the amendment of the EEG (2016/2017), since the change in the subsidy model has subjected wind turbines to renewed and enormous price pressure.

Wind turbines use the wind in the atmospheric boundary layer to generate electricity. The degrees of turbulence prevailing there - determined as the ratio of the standard deviation and the mean value of a time series of the velocity - are 5 to 15 %, in extreme cases even more. Accordingly, a large part of the boundary layer on the wind turbine blade should be in the turbulent flow state. However, this seems to contradict measured performance coefficients (up to 0.54, ENERCON, 2004), which can only be achieved by very high lift-to-drag ratios (over 100, in some cases even values of 200 are advised) of the two-dimensional aerodynamic profiles used. However, such high aerodynamic performance data are only possible if a not too small part ($>$ 20 %) of the boundary layer is in the laminar state, i.e. the transition between laminar and turbulent boundary layer is shifted downstream and consequently the significantly lower frictional resistance of laminar flow prevails on a larger section of the wing.

Direct measurements of the boundary layer on a rotating blade have only recently been carried out repeatedly using modern methods [2, 3, 4]. A theoretical accompaniment of these experimental findings is still pending, since they are neither accessible to a calculation by means of DNS (Direct Numerical Simulation: without any turbulence modeling) nor can they be predicted appropriately with the help of RANS methods (e.g. FLOWer, tau) extended by empirical transition models (e.g. classical e^N method) . In the case of DNS, the gigantic computational effort (proportional to the third power of Re [5]) prevents access, while in the RANS approach with transition models, the validity of the assumptions made is lost due to the high degrees of turbulence in the atmospheric boundary layer.

This includes the condition of small disturbances, which is essential for the linear stability theory and leads to the primary stability theory based on the Orr-Sommerfeld equation. This can be used to predict the so-called natural transition at low turbulence levels starting with the exponential growth of Tollmien-Schlichting waves. According to Reshotko [6], however, at high turbulence levels the initial transition stages (Tollmien-Schlichting waves, Δ-structures) are shortened or even bridged and turbulence spots are formed immediately.

These are strongly non-linearly and lead directly to laminar-turbulent transition, which is then called bypass transition. All theoretical transition models developed for the natural transition in the case of small disturbances are thus invalid.

Plenty of research has been conducted on bypass transition within boundary layers and beneath vortical disturbances on low Re cases using DNS. Various factors have been found to govern the dominant mechanism, for instance: In the absence of a leading-edge and notable pressure gradient effects as in the study by Jacobs and Durbin [7], bypass transition proceeds mainly through the amplification of Klebanoff distortions (streaks). Kendall [8] observed that the growth of T-S waves was influenced by the leading-edge geometry. In Nagaranjan et al. [9] a blunt leading edge led to the formation of instability wave packets at TI levels between 3.5% and 4.5%. These wave packets were amplified downstream leading to turbulence. Today, it is known that the leading edge is the key receptivity site for the penetration of free-stream disturbances as it has the thinnest boundary layer.

The drawback of DNS predictions as mentioned above is their extremely high computational costs. Running DNS for flows with Re numbers in the order of a few million is therefore out of the question in the present day. To overcome this issue, wall-resolved large-eddy simulations (LES) with an adequate resolution of the larger turbulent eddies together with a subgrid-scale (SGS) model can be used. The biggest difference between a LES and RANS is the fact that only a small part of the spectrum (usually isotropic) needs to be modeled, whereas in a RANS the entire spectrum is modelled and hence very model dependent. Sayadi and Moin [10] compared different SGS models and their performance on a coarse and a fine grid based on the predicted skin friction coefficient along a flat plate and showed that dynamic SGS models are capable of predicting the point of transition accurately and independently of the transition scenario.

The Brite-Euram project LESFOIL [11] focused on assessing the feasibility of LES for the computation of the flow around an airfoil at a Reynolds number of two million. It was found that on a very fine mesh, the resolution was sufficient to capture the transition process without numerical forcing. A good agreement with experiments was observed.

To better understand the process of laminar to turbulent transition on wind turbines, experimental studies have been conducted. Within the MexNext project [12] first comparisons between measurements and simulations were carried out and documented on a rotor model with a diameter of 5 m in a wind tunnel. Furthermore, transition was also successfully detected in the collected experimental data [13]:

In Schaffarczyk et al. [3] measurements on a rotor blade of 15 m in length were carried out in the free atmosphere to study the behavior of the boundary layer within a specific zone on the suction side at different operational states. Laminar and turbulent flow was distinguished. In [4] microphone and pressure sensor measurements together with thermographic imaging to study transition on a blade of 45 m length were collected.

A good agreement between both the data of the microphones and the thermographic imaging technique was found. The laminar-turbulent transition location in an associated Reynolds-Averaged Navier-Stokes (RANS) CFD simulation of the transitional flow, wherein an N-factor with respect to Mack's correlation and corresponding to the inflow turbulence intensity was set-up, deviated from the experimental results. Consequently, it was proposed to conduct wall-resolved LES to better understand the transition process within atmospheric turbulence.
According to this long-term goal of running wall-resolved LES with modeled atmospheric inflow turbulence of appropriate length and time scales for a better understanding of the transition modes occurring at Re numbers of several millions, it was decided to step up Re incrementally. The reason is that transitional studies using wall-resolved LES around airfoils for Re numbers in the order of a few million are rarely available. Hence, the present study comprises wall-resolved LES with modeled isotropic atmospheric inflow turbulence carried out at a chord Reynolds number of 100,000 for a 20 % thickness airfoil corresponding to the test section of the aforementioned experiment [4].
An area of particular interest was to look at how much energy of the low-frequency disturbances penetrates into the boundary layer in comparison to a case without any added inflow turbulence and to ultimately determine if a low-frequency cut-off in the frequency spectrum for the determination of the N-factor could be determined.

2 Status of Goals as Defined at the Start of the Project

Below is a list of the original workflow/goals for the project and an updated status next to each point:

- Selection, comparison, parameterisation and implementation of a turbulent wind field generator for describing the inflow turbulence based on the models available at the Kiel UAS (Veers model, Mann model or others, see [14]), Coupling to LES or hybrid LES-URANS code LESOCC. **Status:** The inflow turbulence is generated by the method proposed by Klein et al. [15]. Details on this procedure and its implementation within the LESOCC code are found in the next section.

- Preparations for the LES or hybrid LES-URANS calculations, including the preparation of suitable simulation cases with all boundary conditions, the generation of the required inflow data, grid generation and initial pre-simulations. **Status:** In order to best resolve the transition phenomenon it was decided to conduct wall-resolved LES. This is carried out at three Reynolds numbers of 100k, 500k and 1M. The 100k simulation has been completed and the 500k and 1M simulation are currently being run. The turbulent inflow data for the 500k case has also been generated. For the

1M case, the inflow data will be anisotropic and will be generated, for example, in accordance to the Kaimal formulation (IEC61400-1) resembling atmospheric inflow.

- Carrying out the simulations for different cases (variation of the turbulence, the Reynolds number and the profile shape). For this purpose, local clusters are available for testing at the HSU Hamburg, among others. The very complex actual simulation runs are carried out at HLRN (Hochleitungsrechenzentrum Nord). **Status:** The cases at the three Reynolds numbers as described above are run at 4 - 5 different inflow turbulence levels and at a fixed angle of attack of 4° to match the test section of the aerodynamic Handschuh experiment [4]. Only one fixed angle of attack was chosen due to the limitations of computational resources.

- Evaluation of the simulation data and comparison with experimental data. **Status:** A comparison with experimental data will be carried out for the final simulation cases at a Re of 1M.

- Analysis and evaluation of the results. **Status:** The results are cosntantly being evauated and a list of the publications of the results can be found in Sec 6.

- Considerations on the transferability of the results to the design of wind turbine blades. **Status:** Based on a power spectral analysis of the turbulent kinetic energy penetrating the boundary layer it is possible to analyse the spectrum and determine a low-pass filter for an effective determination of the N factor for the popular e^N method used in RANS simulations. This could be an effective way to use RANS for airfoil design in the future based on an improved understanding of the transition phenomenon in the presence of atmospheric inflow turbulence.

3 Methodology

The simulation methodology relies on a classical wall-resolved large-eddy simulation extended by an inflow generator as explained below. The main features are summarized in Table 1. The filtered three-dimensional, time-dependent Navier-Stokes equations for an incompressible fluid are solved based on a finite-volume method on block-structured grids [16, 17, 18], which is second-order accurate in space and time. The additional subgrid-scale stress tensor mimics the influence of the non-resolved small-scale structures on the resolved large eddies. In the present study, the widely used dynamic version of the classical Smagorinsky model [19] is applied which was introduced by Germano et al. [20] and Lilly [21]. As mentioned in the introduction, the dynamic variant has several advantages compared to the constant coefficient SGS model and is a must for the prediction of transitional flows. The near-wall grid resolution is fine enough to resolve the viscous sublayer. Thus, Stokes no-slip condition is applied at the surface of the airfoil.

Synthetic inflow generators based on a variety of different techniques were suggested in the literature, see, e.g., the review by Tabor and Baba-Ahmadi [22] evaluating the pros and cons of the different techniques. In the present study the digital filter method originally proposed by Klein et al. [15] is applied to generate artificial turbulent inflow data. Presently, the more efficient procedure suggested by Kempf et al. [23] is used, since it reduces the computational effort and memory requirements significantly compared to the original method by Klein et al. [15]. The method relies on discrete linear digital non-recursive filters which depend on certain statistical properties to be defined by the user. These are profiles of the mean velocity and Reynolds stresses and the definition of one integral time scale (T) and two integral length scales (L_y, L_z). These quantities are sufficient to generate artificial turbulence with proper autocorrelations in time and two-point correlations in space. For this purpose, the filter coefficients are multiplied with a series of random numbers characterized by a zero mean and a unit variance. Thereby, the filter coefficients describe the two-point correlations and the autocorrelation of the inflow turbulence. A required three-dimensional correlation between the filter coefficients is achieved by the convolution of three one-dimensional filter coefficients. The cross-correlations between all three velocity components and thus the representation of a realistic inflow turbulence is guaranteed by the application of the transformation by Lund et al. [24].

In the present setup the inflow turbulence is not imposed at the inlet of the computational domain but within the domain using a special source-term formulation developed and validated in [25, 26, 14, 27]. The idea behind the source-term formulation is that it enables the injection of inflow turbulence in sufficiently resolved flow regions. This measure prohibits that it is damped out by numerical dissipation before reaching the region of interest. For external flows as considered in the present study, the inlet region is not resolved by a fine grid, which leads to a strong damping up to a complete cancellation of small flow structures. However, the regions of main interest are the boundary layers and the wake region, where the grid is strongly clustered and thus is sufficiently fine to resolve these structures. Consequently, the injection of the inflow turbulence is done in this region which is two chord lengths upstream of the leading edge of the airfoil. The artificial velocity fluctuations generated by the digital filter method explained above are introduced as source terms directly into the momentum equation. In Schmidt and Breuer [26] the method was shown to guarantee the correct distribution of the autocorrelations. Besides the application to channel flows [26] the source term methodology was also successfully applied to the bluff-body flow past a wall-mounted hemisphere [25] and the flow around the SD7003 airfoil [26, 14, 27]. For more information about the validation of the method, we refer to [26, 14, 27, 25].

Table 1: Finite-volume method and models used for LES.

Property	**Feature**
fluid	incompressible
grid type	curvilinear, block-structured
variable arrangement	cell-centered, non-staggered
discretization of integrals	midpoint rule
interpolation scheme	linear interpolation
accuracy in space	second-order accurate
solution scheme	predictor-corrector time-marching scheme
predictor	low-storage Runge-Kutta scheme
corrector	pressure-correction method
accuracy in time	second-order accurate
pressure-velocity coupling	momentum interpolation technique [28]
turbulence modeling	large-eddy simulation [16, 17, 18]
SGS model	dynamic Smagorinsky model [20, 21]
wall treatment	wall-resolved LES (Stokes no-slip condition)
inflow turbulence	digital filter concept [15, 23]
inflow injection	source-term formulation [25, 26, 14, 27]

4 Results and Discussion

To date, a comprehensive literature survey has been conducted some of which has been outlined in Section 1. The next step was choosing a relevant sub-grid scale model for the LES and an appropriate inflow turbulence generation and insertion method that preserves the generated turbulence and prevents its numerical dissipation as outlined in Section 3. Further, one of the most critical steps was the development of a high quality mesh that was sufficient to resolve the scales that govern the transition process. The dimensions of the grid were chosen based on literature for a wall-resolved LES in addition to performing a grid independence study. Below are some of the results from the first simulation case focusing on the energy penetrating the boundary layer through a power spectral density analysis of the turbulent kinetic energy at 10 % chord and the development of boundary layer streaks and their overall contribution to the transition process as these are the key concepts being studied through this doctoral project.

One of the main objectives of running a PSD analysis was to study the receptivity of the boundary layer in response to increasing TI in addition to it aiding with the analysis of the transition mode. An experiment by Fransson et al. [29] showed that the initial energy in the boundary layer is proportional to the square of the turbulence intensity. Their study included FST between 1.4 and 6.7 % over a flat-plate. A similar analysis was carried out here, with the total energy plotted against the square of TI as seen in

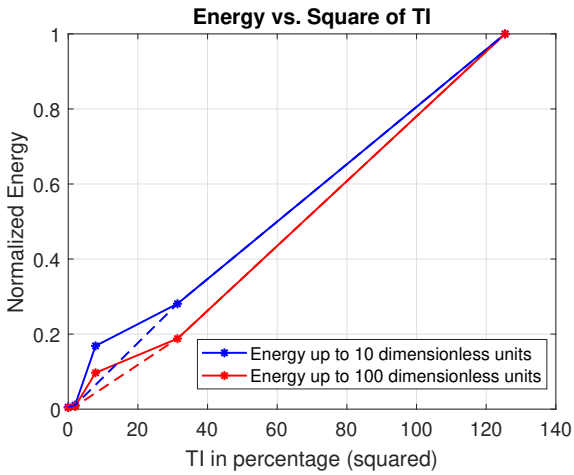

Figure 1: Energy at 10 % chord up to 10 and 100 dimensionless frequency units against the square of the turbulence intensity. The energy is normalized by the value at a TI of 11.2 %.

Fig. 1. Since the boundary layer is receptive to low frequencies as was found through our PSD analysis (See Fig. 2) and as expected from literature, especially near the leading edge, it was decided to plot the total energy including the frequency content up to 10 dimensionless frequency units and at 10 % chord. Since the influence of streaks was observed up to 100 dimensionless frequency units, a second line with the energy including the content up to 100 dimensionless units is plotted. In both cases, ignoring the anomaly at an inflow TI of 2.8 % (the dashed lines ignore this data point), a proportionality via a nearly linear relationship between the energy content and the square of TI is seen. This is in good agreement with the study by Fransson et al. [29].

4.1 Streak analysis

Just as in the study by Hack and Zaki [30] streaks of different sizes, amplitudes and orientations were found in the collected data and at different inflow TI (See Fig. 3). Additionally, the maximum spanwise dimension of the streaks decreased with increasing TI. This is in line with the findings of Zaki et al. [31].

At low inflow turbulence intensities, for example at 1.4 and 2.8 % the time-averaged results (not shown here due to space constraints) indicated that the free-stream turbulence has negligible effects on the onset of separation. However,the instantaneous perturbation fields shown in Fig. 4 show that boundary layer streaks affect the instantaneous separation point. The black rectangular box marks the location of the mean separation region. Instantaneous separation as indicated by the slightly translucent orange iso-surface is shifted upstream in the presence of negative perturbation velocity (dark streaks) and downstream in the presence of positive perturbation velocity (light streaks). These results are in line with earlier studies [32, 31].

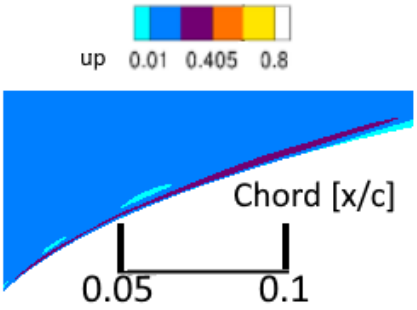

(a) A streak passing through 10 % chord.

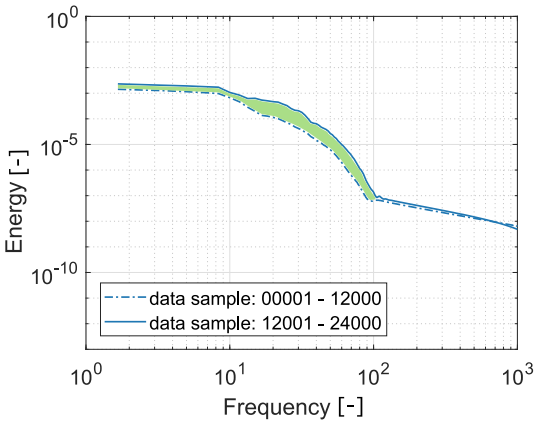

(b) 10 % chord. The dashed line is the PSD prior to the passing of a streak and the solid line is the PSD on the passing of the streak. The shaded region marks the energy difference.

Figure 2: Influence of a boundary layer u' streak on the PSD plot at $TI = 5.6$ %.

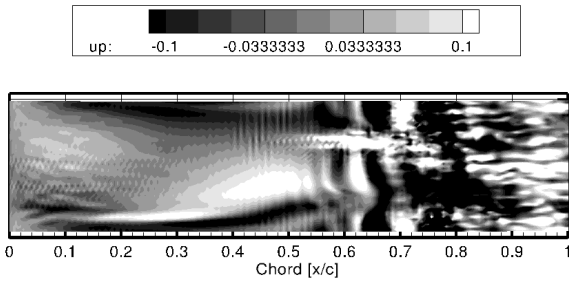

(a) $TI = 1.4$ %

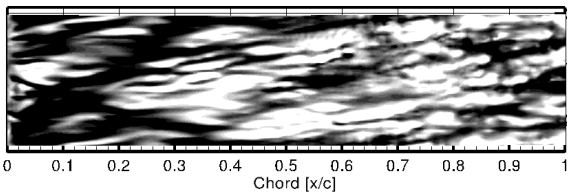

(b) $TI = 11.2$ %

Figure 3: u' boundary layer streaks. Slices are taken at a wall-normal height equal to the displacement thickness at 20 % chord.

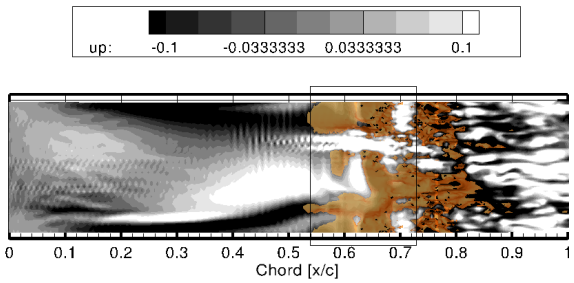

(a) $TI = 1.4$ %

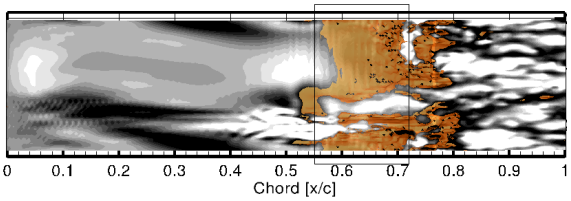

(b) $TI = 2.8$ %

Figure 4: Influence of boundary layer streaks on instantaneous separation. The light and dark streaks represent high- and low-speed streaks, respectively. The orange iso-surface represents instantaneous separation. Slices are taken at a wall-normal distance corresponding to the displacement thickness at 20 % chord.

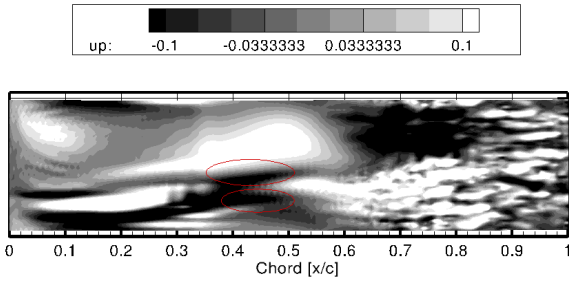

(a) Early stages of overlap between the high and low speed streak. Two different low speed streaks are marked. The lower of the two is the one of interest.

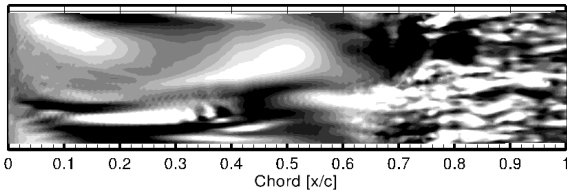

(b) Formation of the varicose instability.

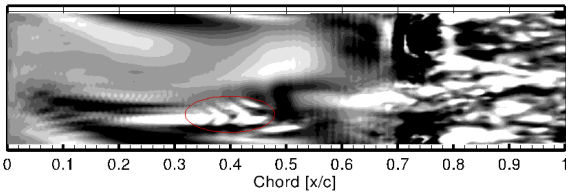

(c) Growth of the instability.

Figure 5: Development of an inner type of instability mode at $TI = 2.8$ %. Contours show the tangential velocity perturbations u'. Each image in this sequence is taken at a dimensionless time period of 0.1 units apart and at a wall-normal distance corresponding to the displacement thickness at 20 % chord.

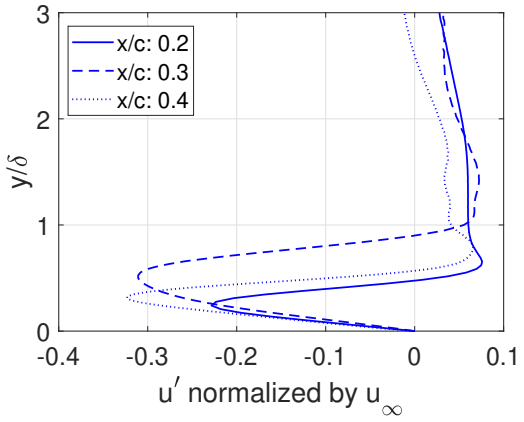

(a) Low-speed streak.

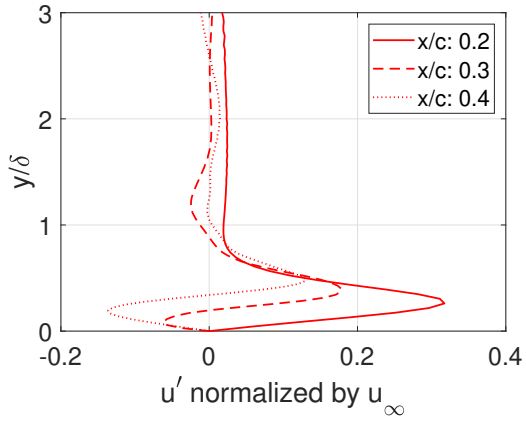

(b) High-speed streak.

Figure 6: u' streaks that lead to the formation of an inner instability at $TI = 2.8$ %.

On account of an adverse pressure gradient (APG), the inner mode of instability [33] was observed at all inflow turbulence intensities. A common scenario attributed to this mode is a local overlap of the trailing edge of a low-speed streak and the leading edge of a high-speed streak which results in the wall-normal velocity profile to become inflectional. This leads to the development of a predominantly varicose instability near the wall. This scenario is the one observed in the present simulations. That is illustrated in Fig. 5 for the case with an inflow TI of 2.8 %. Each image is taken at a dimensionless time period of 0.1 units apart and at a wall-normal distance corresponding to the displacement thickness at 20 % chord. Fig. 5(a) marks the early stages of the overlap between the light high-speed streak and the dark low-speed streak. The overlap takes place with the lower of the two marked streaks. The two streaks have been marked to distinguish them as two separate streaks, a fact that was confirmed by going back in time to the formation of the individual streaks. In Fig. 5(b) the varicose inner instability is seen. At the onset of its formation, the instability has the same spanwise dimension as the parent streak. A similar observation was made in [32]. As the instability develops, the varicose formation becomes clearer and is highlighted in Fig. 5(c). After further 0.1 dimensionless time units, the instability breaks down to form a turbulent spot as seen in Fig. 4(b). This turbulent spot grows and progresses downstream to finally join the fully turbulent flow.

As mentioned above, the origin of the inner instability mode is an overlap of the leading edge of a high-speed streak with the trailing edge of a low-speed streak. An investigation into the formation of the instability must therefore take both streaks into account. Fig. 6 shows the corresponding u' perturbations of the low-speed streak (Fig. 6(a)) which is in time overlapped by the high-speed streak (Fig. 6(b)). For this purpose, consider a slowly moving low-speed streak upstream of which a high-speed streak has formed. The high-speed streak catches up and overlaps the trailing edge of the low-speed streak. This phenomenon causes an inflectional instability. The profiles were generated over a sequence of time steps. The perturbation profile chosen to be plotted is that which possesses the maximum perturbation velocity on the passing of the two relevant streaks.

As seen in Fig. 6(a), the negative perturbation velocity increases as the streak progresses downstream and the streak rises within the boundary layer from 20 to 30 % chord, which is to be expected for a low-speed streak. Even though a slight increase in the negative perturbation velocity is seen at 40 % chord, the streak oddly drops within the boundary layer while it is expected to rise. The time instant of this perturbation velocity plot corresponds to an instant where the varicose instability has already begun to develop upstream of the streak due to shear from the overlap of the high-speed streak. This effectively alters the streak and is a possible cause for this behavior. Fig. 6(b) shows the perturbation velocity on account of the high-speed streak. In this case, the streak has a typical form of a high-speed streak at 20 % chord, but begins to overlap with the low-speed streak at about 30 % chord which is evident from the points of inflection. The streak

amplitude increases up to 20 % chord reaching a value of 32% of the free-stream velocity prior to the development of the instability. Similar values leading to the development of the inner instability are found at other locations and other TI values. This is in agreement with the work by Andersson et al. [34], who observed the critical streak amplitude to be 37 % of the free-stream velocity for the varicose mode.
It must be noted that no evidence was found for an outer type of instability mode. This is attributed to the relatively high APG on the suction side [35], while it is known that a zero- or favorable pressure gradient is decisive for such a mode [7].

5 Conclusions

To further optimize the design of wind turbine blades, the knowledge on the transition process on the blades has to be thoroughly improved. For typical turbulence intensities of atmospheric turbulence it is expected that bypass transition plays an important role. Based on wall-resolved LES predictions the present study should help to expand the knowledge base and to pave the way for the simulation of realistic Reynolds numbers which are currently being carried out.
It is found that the boundary layer is receptive to external disturbances such that the initial energy within the boundary layer is proportional to the square of the turbulence intensity. A similar finding was made in an experimental study by Fransson et al. [29] over a flat plate. In the presence of negative velocity perturbations describing low-speed streaks, separation is found to be shifted upstream. Contrarily, in the presence of positive velocity perturbations according to high-speed streaks separation is shifted downstream. These results are in line with earlier studies [32, 31]. Consequently, it is obvious that boundary layer streaks affect the instantaneous separation point. In the presence of boundary layer streaks, an inner type of instability mode is observed whereby the leading edge of a high-speed streak overlaps the trailing edge of a low-speed streak resulting in an inflectional profile and a varicose mode of instability. This is expected due the APG [35]. The critical streak amplitude was found to be about 32 % of the free-stream velocity. This is in good agreement with the observations by [34], who reported the critical streak amplitude to be 37 % of the free-stream amplitude.
Overall, the results show that the applied methodology of wall-resolved LES with injected inflow turbulence works reliably and provides physically meaningful results. In follow-up studies the Reynolds number will be successively increased in order to understand the transition scenario at the real case under varying inflow conditions.

6 Publications and Conferences

- Contribution of a section about artificial turbulence especially for large-eddy simulations in the book: Schaffarczyk, A. P. (2020). Introduction to wind turbine aerodynamics (2nd ed.). Cham, Switzerland: Springer Nature.

- Lobo, B. A., Schaffarczyk, A. P., and Breuer, M.: Investigation Into Boundary Layer Transition Using Wall-Resolved LES and Modeled Inflow Turbulence, Wind Energ. Sci. Discuss. [preprint], https://doi.org/10.5194/wes-2021-30, in review, 2021.

- Lobo, B. A., Schaffarczyk, A. P., and Breuer, M.: Influence of Low-Frequency Components of Free-Stream Turbulence on Boundary Layer Transition using Wall-Resolved Large-Eddy Simulations. Wind Energy Science Conference, Hannover. May 25 - 28, 2021.

- Contribution to a section in the IEA Task 29, Phase IV: J.G. Schepers et al. IEA Wind TCP Task 29, Phase IV: Detailed Aerodynamics of Wind Turbines, 2021 https://doi.org/10.5281/zenodo.4817875

Acknowledgement

A special thanks to EKSH and in particular Dr. Klaus Wortmann for their support through the EKSH Promotionsstipendium that has made this work possible. The project continues with the simulation and post-processing of the data at a Reynolds number of 500k and 1M. The simulations would also not be possible without support from the HLRN supercomputing network.

References

[1] Ivan Komusanac, Guy Brindley, and Daniel Fraile. *Wind Energy in Europe in 2019 – Trends and Statistics*. Tech. rep. Wind Europe, 2020.

[2] Helge Madsen et al. "The DAN-AERO MW Experiments". In: *48th AIAA Aerospace Sciences Meeting Including the New Horizons Forum and Aerospace Exposition*. Reston, Virigina: American Institute of Aeronautics and Astronautics, 2010.

[3] A. P. Schaffarczyk, D. Schwab, and M. Breuer. "Experimental Detection of Laminar–Turbulent Transition on a Rotating Wind Turbine Blade in the Free Atmosphere". In: *Wind Energy* 20 (2017), pp. 211–220.

[4] Torben Reichstein et al. "Investigation of laminar-turbulent transition on a rotating wind-turbine blade of multi-megawatt class with thermography and microphone array". In: *Energies* 12.11 (2019), p. 2102.

[5] Steven B. Pope. *Turbulent Flows*. Cambridge: Cambridge University Press, 2000.

[6] E Reshotko. "Paths to Transition in Wall Layers". In: *Advances in Laminar-Turbulent Transition Modelling, Report NATO Research and Technology Organisation, RTO-EN-AVT151*. 2009, pp. 1–8.

[7] R. G. Jacobs and P. A. Durbin. "Simulations of bypass transition". In: *J. Fluid Mech.* 428 (2001), pp. 185–212.

[8] J M Kendall. "Studies on laminar boundary-layer receptivity to freestream turbulence near a leading edge". In: *Proc. of the Symp., ASME and JSME Joint Fluids Engineering Conference, 1st, Portland, OR, June 23-27, 1991 (A92-36003 14-34). New York, American Society of Mechanical Engineers*. 1991, pp. 23–30.

[9] S. Nagarajan, S. K. Lele, and J. H. Ferziger. "Leading-edge effects in bypass transition". In: *J. Fluid Mech.* 572 (2007), pp. 471–504.

[10] T. Sayadi and Parviz Moin. "Predicting natural transition using large eddy simulation". In: *Annual Research Briefs 2011*. Center for Turbulence Research, 2011, pp. 97–108.

[11] Christopher P. Mellen, Jochen Fröhlich, and Wolfgang Rodi. "Lessons from LESFOIL Project on Large-Eddy Simulation of Flow Around an Airfoil". In: *AIAA J* 41.4 (2003), pp. 573–581.

[12] K Boorsma et al. *Final report of IEA Wind Task 29 Mexnext (Phase 3)*. Tech. rep. ECN-E–18-003. ECN Publications, 2018.

[13] B. A. Lobo, K. Boorsma, and A. P. Schaffarczyk. "Investigation into boundary layer transition on the MEXICO blade". In: *J. Physics: Conference Series* 1037 (2018), p. 052020.

[14] M. Breuer. “Effect of Inflow Turbulence on an Airfoil Flow with Laminar Separation Bubble: An LES Study”. In: *J. Flow, Turbulence and Combustion* 101.2 (2018), pp. 433–456.

[15] M. Klein, A. Sadiki, and J. Janicka. “A digital filter based generation of inflow data for spatially–developing direct numerical or large–eddy simulations”. In: *J. Comput. Phys.* 186 (2003), pp. 652–665.

[16] M. Breuer. “Large–eddy simulation of the sub–critical flow past a circular cylinder: Numerical and modeling aspects”. In: *Int. J. Numer. Meth. Fluids* 28.9 (1998), pp. 1281–1302.

[17] M. Breuer. “A challenging test case for large–eddy simulation: High Reynolds number circular cylinder flow”. In: *Int. J. Heat Fluid Flow* 21.5 (2000), pp. 648–654.

[18] M. Breuer. *Direkte Numerische Simulation und Large–Eddy Simulation turbulenter Strömungen auf Hochleistungsrechnern.* Habilitationsschrift, Universität Erlangen–Nürnberg, Berichte aus der Strömungstechnik. Shaker Verlag, Aachen, 2002.

[19] J. Smagorinsky. “General Circulation Experiments with the Primitive Equations, I, The Basic Experiment”. In: *Monthly Weather Review* 91 (1963), pp. 99–165.

[20] M. Germano et al. “A dynamic subgrid–scale eddy viscosity model”. In: *Phys. Fluids A* 3 (1991), pp. 1760–1765.

[21] D. K. Lilly. “A proposed modification of the Germano subgrid–scale closure method”. In: *Phys. Fluids A* 4 (1992), pp. 633–635.

[22] G.R. Tabor and M.H. Baba–Ahmadi. “Inlet conditions for large–eddy simulation: A review”. In: *Computers & Fluids* 39 (2010), pp. 553–567.

[23] A. Kempf, S. Wysocki, and M. Pettit. “An efficient, parallel low–storage implementation of Klein’s turbulence generator for LES and DNS”. In: *Computers & Fluids* 60 (2012), pp. 58–60.

[24] T. S. Lund, X. Wu, and K. D. Squires. “Generation of Turbulent Inflow Inlet Data for Spatially–Developing Boundary Layer Simulations”. In: *J. Comput. Phys.* 140 (1998), pp. 233–258.

[25] G. De Nayer et al. “Enhanced Injection Method for Synthetically Generated Turbulence within the Flow Domain of Eddy–Resolving Simulations”. In: *Computers and Mathematics with Applications* 75.7 (2018), pp. 2338–2355.

[26] S. Schmidt and M. Breuer. “Source Term based Synthetic Turbulence Inflow Generator for Eddy–Resolving Predictions of an Airfoil Flow including a Laminar Separation Bubble”. In: *Computers & Fluids* 146 (2017), pp. 1–22.

[27] M. Breuer and S. Schmidt. "Effect of Inflow Turbulence on LES of an Airfoil Flow with Laminar Separation Bubble". In: *ERCOFTAC Series, Direct and Large-Eddy Simulation XI, 11th Int. ERCOFTAC Workshop on Direct and Large–Eddy Simulation: DLES-11, Pisa, Italy, May 29–31, 2017*. Ed. by M. V. Salvetti et al. Vol. 25. Springer Nature Switzerland AG, 2019, pp. 351–357.

[28] C. M. Rhie and W. L. Chow. "A Numerical Study of the Turbulent Flow Past an Isolated Airfoil with Trailing Edge Separation". In: *AIAA J.* 21 (1983), pp. 1525–1532.

[29] J. H. M. Fransson, M. Matsubara, and P. H. Alfredsson. "Transition induced by free-stream turbulence". In: *J. Fluid Mech.* 527 (2005), pp. 1–25.

[30] M. J. P. Hack and T. A. Zaki. "Streak instabilities in boundary layers beneath free-stream turbulence". In: *J. Fluid Mech.* 741 (2014), pp. 280–315.

[31] T. A. Zaki et al. "Direct numerical simulations of transition in a compressor cascade: The influence of free-stream turbulence". In: *J. Fluid Mech.* 665 (2010), pp. 57–98.

[32] A. D. Scillitoe, P. G. Tucker, and P. Adami. "Large eddy simulation of boundary layer transition mechanisms in a gas-turbine compressor cascade". In: *J. Turbomachinery* 141 (2019), p. 061008.

[33] Nicholas J Vaughan and Tamer A Zaki. "Stability of zero-pressure-gradient boundary layer distorted by unsteady Klebanoff streaks". In: *J. Fluid Mech.* 681 (2011), pp. 116–153.

[34] Paul Andersson et al. "On the breakdown of boundary layer streaks". In: *J. Fluid Mech.* 428 (2001), pp. 29–60.

[35] Matthieu Marquillie, Uwe Ehrenstein, and Jean-Philippe Laval. "Instability of streaks in wall turbulence with adverse pressure gradient". In: *J. Fluid Mech.* 681 (2011), pp. 205–240.